Cut-and-connect of two antiparallel vortex tubes

By MOGENS V. MELANDER† AND FAZLE HUSSAIN‡

Motivated by our early conjecture that vortex cut-and-connect plays a key role in mixing and production of turbulence, helicity and aerodynamic noise, we have studied the cross-linking of two antiparallel viscous vortex tubes via direct numerical simulation. The Navier-Stokes equations are solved by a dealiased pseudo-spectral method with 64^3 grid points in a periodic domain for initial Reynolds numbers Re $(= \Gamma/\nu)$ up to 1000; Γ is the circulation and ν is the kinematic viscosity. The vortex tubes are given an initial sinusoidal perturbation to induce a collision and keep the two tubes pressed against each other as annihilation continues. Cross-sectional and wire plots of various properties depict three stages of evolution: (I) *Inviscid* induction causing vortex cores to first approach and form a contact zone with a dipole cross-section, and then to *flatten* and *stretch*. (II) Vorticity annihilation in the contact zone accompanied by *bridging* between the two vortices at both ends of the contact zone due to a collection of cross-linked vortex lines, now orthogonal to the initial vortex tubes. The direction of dipole advection in the contact zone reverses. (III) *Threading* of the remnants of the original vortices in between the bridges as they pull apart. We show the crucial stage II to be a simple consequence of vorticity annihilation in the contact zone, link-up of the un-annihilated parts of vortex lines, and stretching and advection by the vortex tube swirl of the cross-linked lines, which accumulate at stagnation points in front of the annihilating vortex dipole. We claim that bridging is the essence of any vorticity cross-linking and that annihilation is sustained by stretching of the dipole by the bridges.

Induction by the bridges reverses the curvature of the dipole vortices and the direction of their motion. This reversal would arrest annihilation, were it not for the fact that the stretching by the bridges sustains annihilation, albeit at a slower rate. The bridges pull away from each other by self induction while the stretched remnants (i.e. threads) of the initial vortex dipole decay. The threads decay very slowly both because of the balance between stretching and viscous diffusion, and because of the absence of induction pressing the threads against each other. Threading, in addition to bridging, is an integral part of reconnection contributing to mixing and enstrophy cascade.

Vortex reconnection details are found to be insensitive to asymmetry. Modeling of the reconnection process is briefly examined. We also examine the 3D spatial details of scalar transport (at unity Schmidt number), enstrophy production, dissipation and helicity.

---

† Southern Methodist University
‡ University of Houston

1. Introduction

Since turbulent flow can be viewed as a tangle of vortices, vortex dynamics is an attractive and tractable avenue for understanding fundamental turbulence mechanisms. The discovery of large-scale organized vortical motions, popularly called "coherent structures" (CS), in flows which were heretofore regarded as fully random (Cantwell 1981; Lumley 1981; Kim & Moin 1986), has fostered the concept that CS dominate turbulence phenomena such as transports of heat, mass and momentum, combustion and chemical reaction, and generation of drag and aerodynamic noise, and that these phenomena can be managed by active and passive manipulation of CS formation and interactions (Hussain & Husain 1987). Vortex dynamics can be an effective tool in understanding CS topology and dynamics in unexcited and excited flows, especially in the absence of any theoretical framework for CS.

Inviscid vortex dynamics is particularly suited for studying CS evolution and interaction as CS dynamics is essentially inviscid and we define CS in terms of vorticity (Hussain 1980, 1986). Inviscid vortex dynamics are governed by the conservation theorems of Kelvin and Helmholtz and the Biot-Savart induction equation. In the case of thin vortices with small curvature, the local induction approximation provides a considerable simplification in analysis and gathering intuition regarding the instantaneous self and mutual inductions of vortical structures. Two particular idealizations have found extensive use: filaments and point vortices. Representation of vortices by filaments is appropriate under some constraints and has been dealt with by many researchers (Leonard 1980; Siggia 1985; Schwarz 1985). For a discussion of motions of point vortices see Aref (1982). A generalized point vortex model for 2D vortex merger has been given by Melander *et al.* (1986, 1988). Many interesting phenomena have been studied by inviscid vortex dynamics: entanglement (Hopfinger *et al.* 1982; Takaki & Hussain 1984), short wave instability (Widnall *et al.* 1974; Saffman 1978), Tkachenko waves (Andreck & Glaberson 1982), for example.

Viscous vortex interactions can be classified into two categories: augmentation and annihilation of circulation. Pairing and entanglement usually produce accumulation of circulation due to merger of like-signed vortices, although pairing of opposite-signed vortices has been observed (Hussain 1983). Annihilation of circulation, for which viscosity is essential, can occur with and without reconnection. Head-on collision of viscous vortex rings (Kambe & Minota 1983) is an example of annihilation without reconnection and has been numerically simulated in a companion study (Stanaway *et al.* 1988). Examples of annihilation with reconnection include aircraft trailing vortices (Crow 1970), pinching-off in hairpin tips in boundary layers (Moin *et al.* 1986), fusion of two parallel adjacent vortex rings (Oshima & Asaka 1977; Kida *et al.* 1988), two colliding rings at arbitrary orientations (Schatzle 1987), splitting of an elliptic jet into two (Hussain & Husain 1987), collision of two antiparallel vortex filaments (Meiron *et al.* 1988), etc. Note that Meiron *et al.* use two zero-circulation vortices—an unnecesary complication not present in our study. The studies of a trefoil vortex (Kida & Takaoka 1987) and of two colliding orthogonal vortex tubes (Zabusky & Melander 1988) also fall in this general category; the motions in both these cases, however, are extremely complex and not

easily understood.

1.1. *Motivation*

The cut-and-connect process, also called cross-linking or reconnection, is of general interest as an example where topology is not preserved. However, there are particular motivations for the present study. Following Laufer's (1974) proposal that vortex pairing was the dominant factor in jet noise generation, we argued that pairing was an unlikely cause in practical jets, which involve very little pairing, and that it was the breakdown of vortical structures which produced most noise in jets. We then proposed cross-linking as the specific mechanism involved (Hussain 1983) and then further proposed it to be responsible for mixing, turbulence production and helicity generation (Hussain 1986). Although we had no measurements (of vorticity) to support our claim regarding the role of vortex cut-and-connect, we presented an idealized model which not only shed some light on the mechanism but also produced far-field jet noise predictions in qualitative agreement with experiments (Takaki & Hussain 1985).

The second motivation for a rigorous study of the cross-linking process is to obtain a clear understanding of the role of viscosity. In the absence of viscosity, vortex lines are material and thus cannot cut and connect, according to the theorems of Kelvin and Helmholtz. It is clear that viscosity is crucial to cross-linking, as emphasized in the analysis of Takaki & Hussain (1985). They coined the phrase 'cut and connect' to emphasize the topology-changing nature of the event, although the event, a consequence of viscous diffusion, obviously involves no cutting (or breaking) whatsoever of vortex lines. There are many who still feel viscous effects are irrelevant to cross-linking (Benjamin 1985). For example, Melander & Zabusky (1988) suggest that viscous effects are not operative at large Re during several convective intervals.

Different mechanisms of cross-linking are implied in different studies. Siggia & Pumir (1985) and Ashurst & Meiron (1987) proposed "tangling and collapse" of vortices. In their idealized analysis, Takaki & Hussain (1985) transformed the cut-and-connect problem into an equivalent problem where cross-linking occurs smoothly (but very rapidly) as a viscous diffusion phenomenon. Kida & Takaoka's (1987) simulation suggests that high-vorticity fingers ejected from the main vortices, get elongated and then connected with other fingers to form "bridges". (Note that this mechanism, despite the same name, is quite different from the bridging mechanism we discuss here). Melander & Zabusky's (1988) simulation suggests the formation of hairpin vortices, which are pulled out from the outer layer fluid of colliding vortices and then intensified, causing subsequent entanglement. As will be seen here, the mechanism we observe and analyze is indeed quite different—it is truly viscous. Viscous annihilation is a precondition for our bridging. Kida & Takaoka's 'bridging', as Melander & Zabusky's mechanism, is by mutual induction and does not require viscosity for initiation. Their mechanism may occur at high Re, but whether it will occur on an inviscid time scale at high Re is unclear.

Another aspect that remains unresolved is the characteristic time scale of the phenomenon. Takaki & Hussain (1985) emphasized that viscosity was crucial, yet

its effect was indirect. They claimed that the cut-and-connect happened rapidly in a time scale $\mathcal{O}(\sigma^2/\Gamma)$, where σ is the instantaneous core size. Based on his data, Schatzle (1987) proposed two time scales $\sigma/(e\nu)^{1/2}$ and $\sigma^2/(\Gamma\nu)^{1/2}$ in terms of strain rate e and circulation Γ. The strain rate is set by Γ in ways that remain unclear. He also quotes a time scale of $(1/2e)\log(\sigma^2 e/\nu)$ suggested to him by Saffman and Leonard. He was unable to indicate a clear preference between these three, as all three gave values comparable to those in his experiment. Meiron *et al.* (1988) have proposed a time scale of $\log(\Gamma/\nu)/2e$. Melander & Zabusky (1988) also suggest that if there is balance between strain and dissipation, then the time scale $\sim \log(\Gamma/\nu)$.

Singularity of the Navier-Stokes equation is another reason why cross-linking is particularly interesting. Do solutions of the incompressible Navier-Stokes equation (in the limit $\nu \to 0$) blow up in finite time? Recent studies by Siggia (1985) and Siggia & Pumir (1985) suggest singularity of the Euler solutions in finite time. (Also, Pumir & Siggia (1987) claim that there is a singularity in the Navier-Stokes equation at sufficiently high Re). However, their study involving inviscid vortex filaments cannot be viewed as conclusive as it is not clear if the solutions obtained by vortex filament simulations correspond to solutions of Euler equations near the time of singularity, including the fact that their simulations do not consider strong core deformation which, as we will see herein, is a crucial factor in cross-linking. The singularity issue is not addressed in the present paper but is discussed in a concurrent study elsewhere (Kerr & Hussain 1988).

1.2. *Objective*

It is clear from the above brief review that the cross-linking mechanism and the time scales involved are far from being understood. The need for modeling the event cannot be overemphasized. However, modeling should be based on carefully digested observations—not a popular practice! Schatzle (1987) proposed that further careful experiment and numerical simulation were needed. Meiron *et al.* (1988) also concluded, as we did, that the present state of understanding of cross-linking was extremely poor and that further study was warranted.

Before stating our objective, we must explain why we studied antiparallel vortices and why numerically.

In spite of numerous flow visualization studies of reconnection, especially in rings, there is practically no quantitative measurement, except the recent one by Schatzle (1987). Unfortunately, his measurements involve ensemble averaging, assuming identical details of the cross-linking process in space and time in successive runs of the same event by repeated experiments; in addition to the inherent smoothing in such ensemble averaging (along with spatial averaging used by him), his measurements are limited in resolution and also by the fact that data were taken in one plane only. This clearly misses 'bridging' which we claim here to be the essence of cross-linking. We need instantaneous data over the 3D field with adequate resolution. Pending further development in measurement technology (now in progress in our laboratory), experimental methods cannot now do much better. However, supercomputer simulation can provide time evolution of reconnection in 3D and with adequate resolution, especially at low Re.

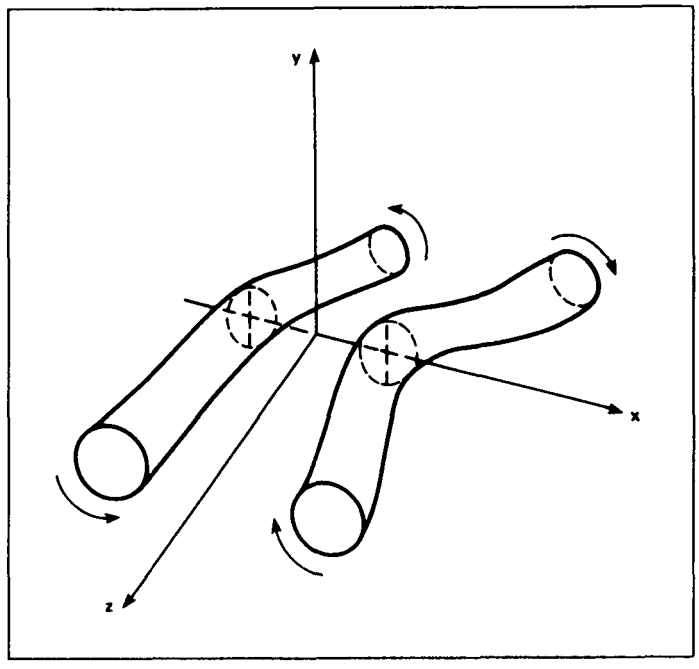

FIGURE 1. Schematic of the initial vortex tubes and coordinates.

The simulation of Kida & Takaoka (1987) of a trefoil and of Melander & Zabusky (1988) of two colliding orthogonal vortex tubes show that the local interaction, which involves entanglement and cross-linking, is extremely complex, even virtually intractable. However, we know that two vortex filaments of arbitrary orientations will tend to become antiparallel by mutual induction as they approach each other. This was also apparent in the simulations of Siggia (1985) and Pumir & Siggia (1987). Thus, one can focus on the details of cross-linking by considering the simple case of antiparallel vortex tubes. In order to aid the collision and annihilation, so that the two vortex tubes press against each other for sustained annihilation, they were given parallel sinusoidal perturbations, the planes of the two cosine waves being inclined to each other (figures 1 & 2).

The objectives of this study were to:

i) Obtain a clean simulation of two antiparallel vortex tubes with initially circular cross-section.

ii) Explain the detailed mechanism of cross-linking by examining the processes of annihilation, motion of dipole and bridging.

iii) Explain the origin and role of bridging.

iv) Identify the time scale of cross-linking.

v) Explain the final stage of cross-linking (that is, is reconnection complete or is there debris left?).

vi) Determine sensitivity of cross-linking to asymmetry.

vii) Study topology and dynamics of cross-linking by considering the 3D fields of properties, including enstrophy production, dissipation, helicity, scalar transport

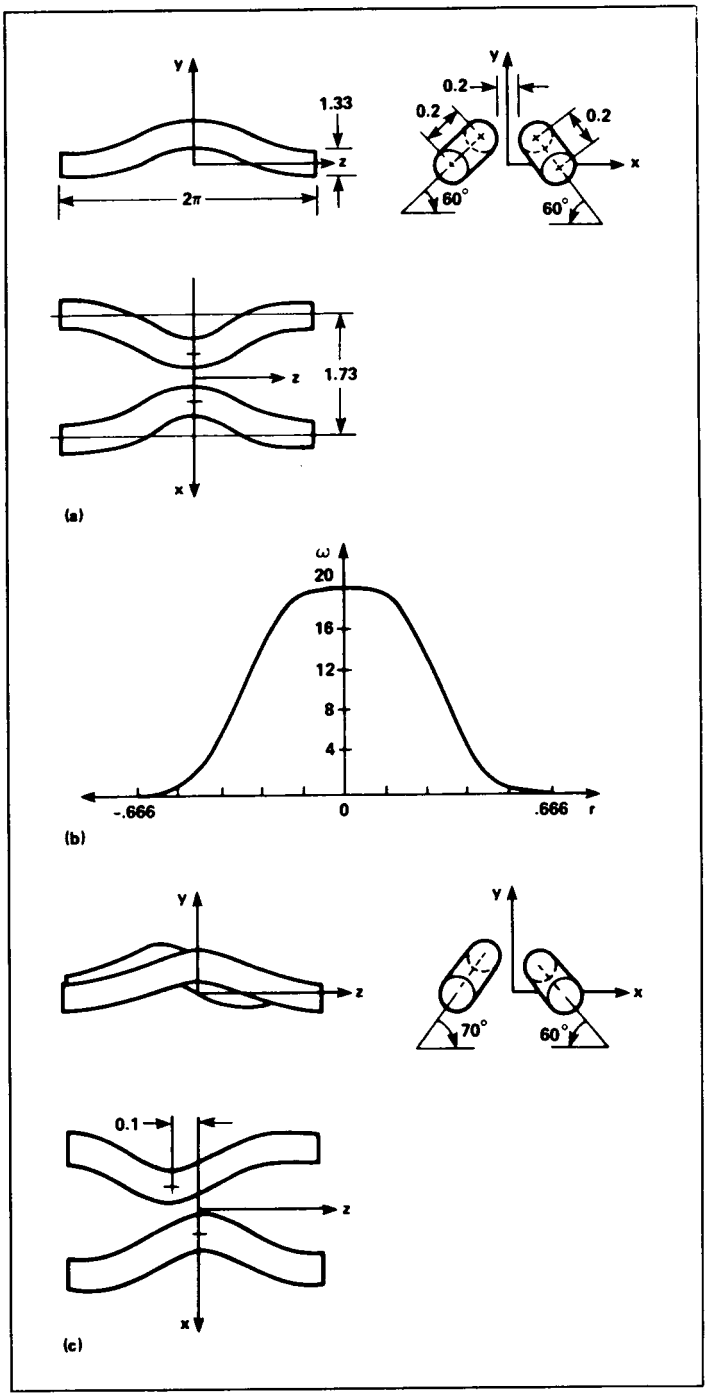

FIGURE 2. (a) Three views of the initial state for symmetric computation; (b) initial vorticity distribution within the core; (c) initial configuration for asymmetric computation.

etc.

viii) Suggest modeling of the cross-linking: core deformation and head-tail formation, bridging and threading.

2. Simulation method

Our numerical method, used for solving the Navier-Stokes equation in a cube with periodic boundary conditions, is a pseudo-spectral (Galerkin) method with a fourth-order, predictor-corrector for time stepping. Dealiasing is performed by a 2/3-spherical truncation in k-space. The choice of periodic boundary conditions is justified by the fact that cross-linking is a strong local vortex interaction, which is insensitive to weak nonlocal effects. In a different study by Melander & Zabusky (1988, and private communication) the influence of adjacent boxes was studied, and it was found that the effect is inconsequential.

The initial conditions consist of two antiparallel vortices with a sinusoidal perturbation as shown in figure 2. Each vortex (unperturbed) has a circular cross-section with an initial vorticity profile given by,

$$\omega(r) = \begin{cases} 20\,[1 - f(r/0.666)] & r < 0.666 \\ 0 & r \geq 0.666 \end{cases}, \qquad f(\eta) = \exp\left[-K\eta^{-1}\exp(1/(\eta-1))\right], \quad K = \frac{1}{2}\exp(2)\log(2). \tag{1}$$

After the perturbation is applied, this defines a vorticity field $\boldsymbol{\omega}_{\text{in}}$ which may not be divergence free. In order to ensure a divergence-free vorticity field we first calculated the curl of the specified initial vorticity field,

$$\boldsymbol{\eta} = \nabla \times \boldsymbol{\omega}_{\text{in}}, \tag{2}$$

and then find a modified vorticity field $\boldsymbol{\omega}$ by inverting the following two equations,

$$\boldsymbol{\eta} = \nabla \times \boldsymbol{\omega}, \qquad \nabla \cdot \boldsymbol{\omega} = 0, \tag{3}$$

which guarantee divergence-free vorticity field. This inversion makes a slight adjustment in $\boldsymbol{\omega}_{\text{in}}$ without introducing any noticeable vorticity away from the core (i.e., $r > 0.666$).

The total circulation in the box vanishes due to the symmetry in the initial condition. Therefore, there is no need to use vortices whose individual circulations vanish, as is the case in the initial conditions used by Meiron *et al.* (1988).

3. Observations

Figure 1 shows the schematic of the initial vortices along with the coordinates x, y, z. For the sake of clear identification let us distinguish the two planes of symmetry: we will call the xy-plane the *symmetric* plane and yz-plane the *dividing* plane. Figure 2(a) shows three views of the initial configuration of the vortex pair. Note that the computational domain contains one full wave with the cross-linking zone

at the center of the domain. The two sine waves are inclined to each other at 60° so that these two vortices move by self induction along the local binormal (Batchelor 1967; p. 510) to make contact at the center and that they remain pressed against each other as the annihilation continues. The initial inclination angle, the amplitude of the sine wave and the core separation were chosen to shorten the time required to make contact. The vortex cores of circular cross-section are centered along the sine wave. The vorticity distribution (figure 2b) has compact support so that, unlike the Gaussian distribution which has tails extending to infinity, there is no vorticity outside the core boundary (i.e. $r = 0.666$). This is somewhat of an artifact, but introduced to make the cross-linking process clean, focused at the contact zone, and tractable. Without this, vorticity cross-linking would occur everywhere along the dividing plane and would cloud the central issue. This initial configuration was obtained as the optimum after some iteration. Figure 2(c) shows the initial configuration used to determine the effects of asymmetry on the evolution of the cross-linking process. Note that this configuration is asymmetric in all directions. In this paper all figures will be for the symmetric simulation only. We will merely mention the effect of asymmetry.

The results will be discussed at the times $t = 0, 1, 2, 3, 3.75, 4.5$ and 6 where t is time t^* nondimensionalized by initial peak vorticity, i.e. $t = t^*|\omega|_{\max}(0)/20$.

Figures 3(a–g) show surfaces of $|\omega| = 0.3|\omega|_{\max}(0)$. The corresponding vorticity contours in the symmetric (xy) plane are shown in figures 4(a–g). Between the first two frames, self-induction brings the two cores closer and they deform from being circular. At $t = 2$ the cores are siginificantly flattened. The two vortices contact each other at some time between $t = 2$ and 3. Note that by $t = 3$ the formation of the characteristic head-tail structure of a vortex dipole is clear. Up to this point the vorticity distribution within each is not unlike that in the case of head-on collision of circular vortex rings studied by Stanaway *et al.* (reported herein). Note that the two cores move upward by mutual induction. Until this time, the vorticity in the dividing (yz) plane is zero, but not now. The vorticity contours in this plane at $t = 3, 3.75, 4.5$ and 6 are shown in figures 5 (a–d), respectively.

As will be discussed in the next section, annihilation of vorticity in the symmetric (xy) plane is accompanied by appearance of orthogonal vorticity in the dividing (yz) plane as a result of cross-linking. The amount of circulation lost by annihilation is precisely the amount of circulation appearing in the dividing (yz) plane. So the amount of circulation annihilated at $t = 3$ is apparent from that in figure 5(a).

The most dramatic change in the topology happens between $t = 3$ and 3.75. Between these two times significant annihilation has happened. There is also the appearance of two humps in figure 3(e) connecting the two vortex tubes across the initial contact point. These two, which we call "bridges", are direct consequences of annihilation and resulting reconnection, and will be discussed later.

The circulation Γ in one half of the xy plane is shown in figure 6 as a function of time. Note that most of the circulation decay by annihilation has already taken place by $t = 3.75$. The same amount of circulation has accumulated in the yz plane (figure 5b). By $t = 4.5$, 70% of the circulation has been annihilated. Because of

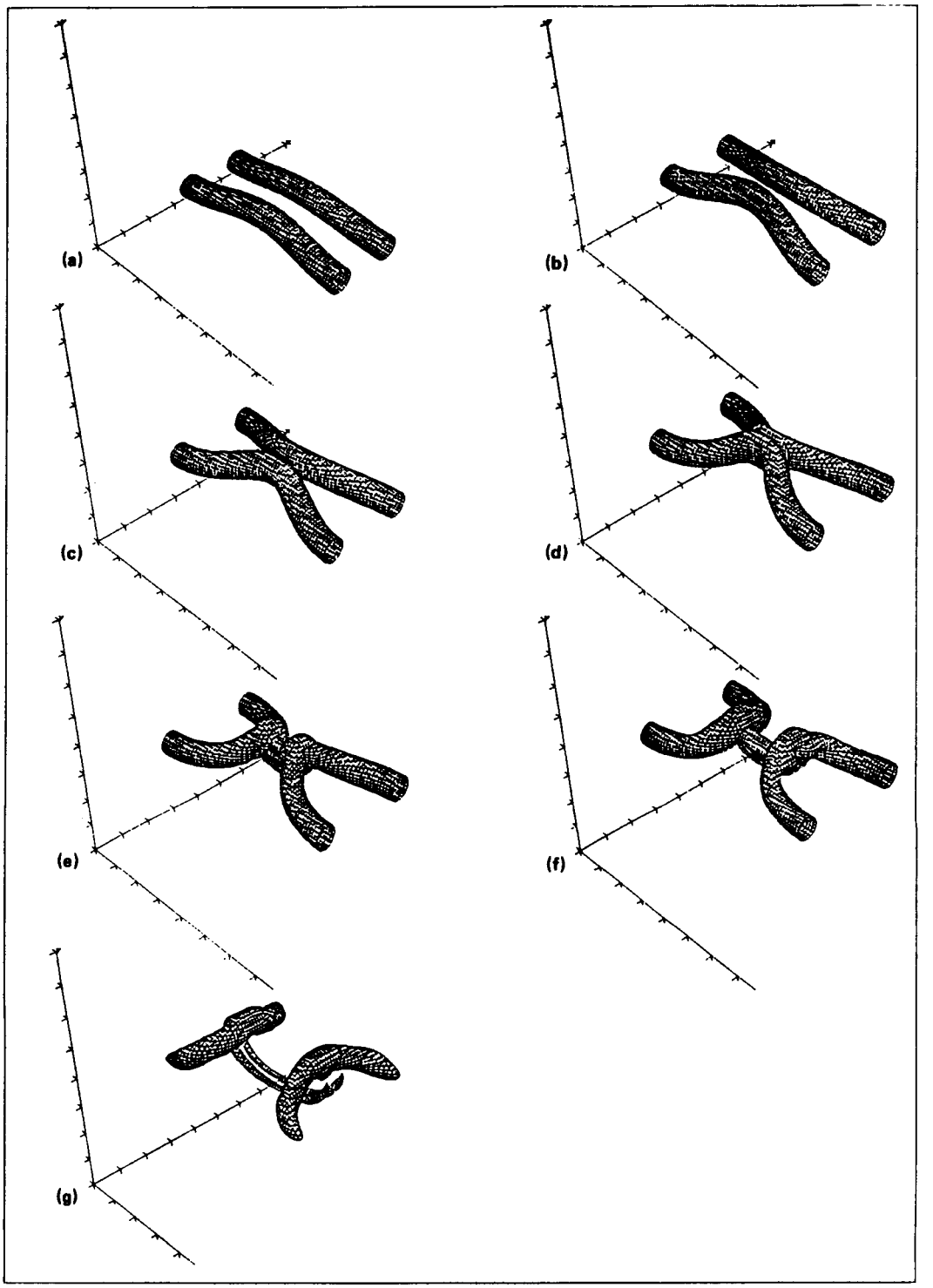

FIGURE 3. Wire plots of $|\omega|$ surface at 30% of initial peak vorticity. (a) $t = 0$; (b) $t = 1$; (c) $t = 2$; (d) $t = 3$; (e) $t = 3.75$; (f) $t = 4.5$; (g) $t = 6$.

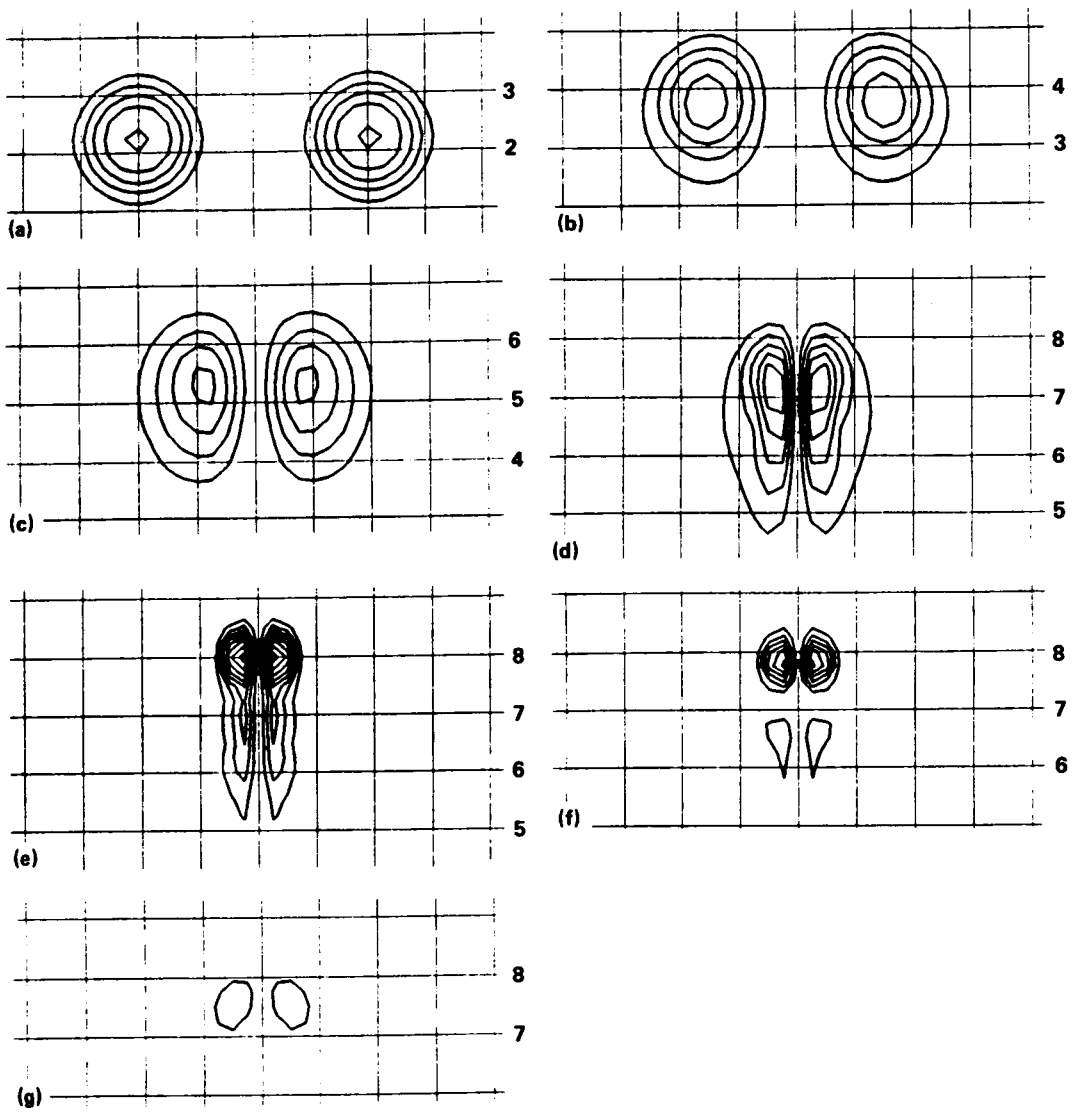

FIGURE 4. Contours of vorticity normal to the symmetric (xy) plane at times corresponding to figures 3(a–g). The grid is four times coarser than the computational mesh. The numbers on the right indicate the dipole motion in the y direction.

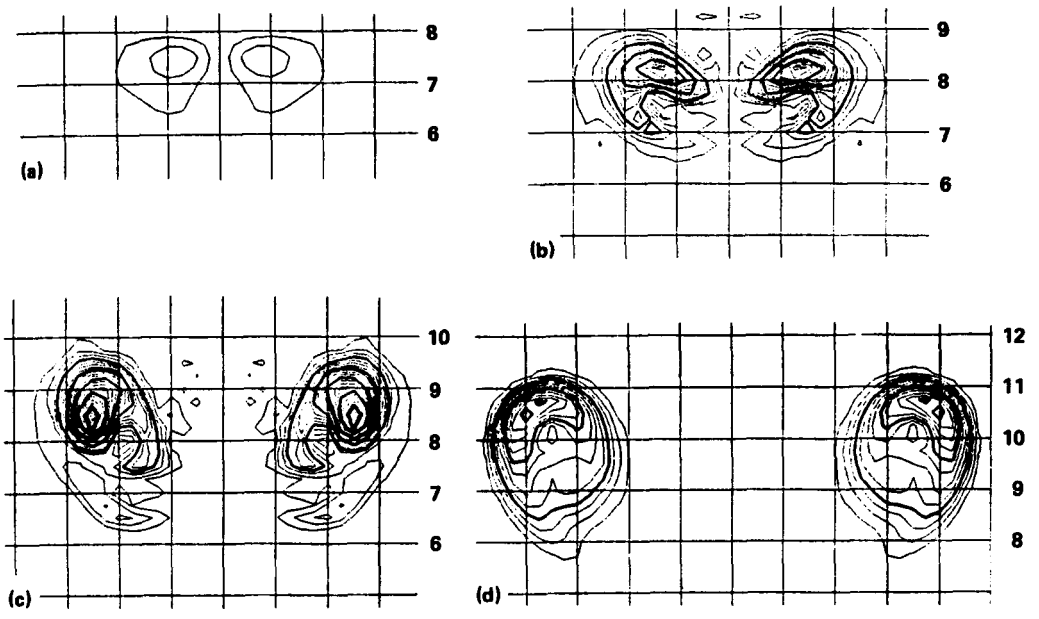

FIGURE 5. Contours of ω_x in the dividing (yz) plane. Contour spacing: thin lines, $\Delta\omega_x = 1$; thick lines, $\Delta\omega_x = 4$. (a) $t = 3$; (b) $t = 3.75$; (c) $t = 4.5$; (d) $t = 6$.

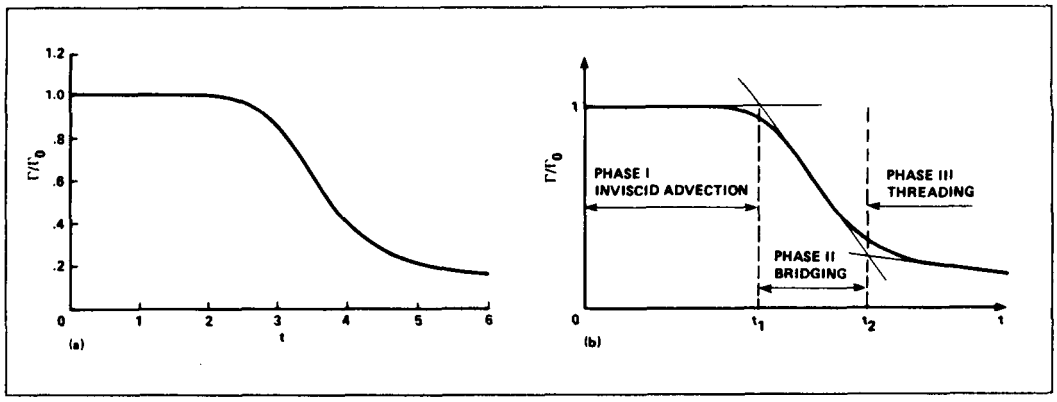

FIGURE 6. (a) Circulation as a function of time in one half of the symmetric (xy) plane; (b) Phases and time scales of reconnection.

higher vorticity concentration, the annihilation is much more between the heads than between the tails. The head moves ahead leaving the tail behind (figures 3f, 4f). The tail decays more by viscous diffusion than by annihilation. The reconnected vortex configuration at $t = 3.75$ is such that the bridges move apart by self-induction. An interesting point to observe is that the bridges pull apart much faster than the rate at which the vortices initially approach each other (compare figures 4 and 5). This is because the bridges, looking like curved hairpins, have much larger curvature and therefore higher self-induction velocities. The two bridges now induce a downwash in the contact zone which reverses the direction of motion of the vortex dipole. As the two bridges pull apart they stretch the dipole into two slender threads. The two threads now undergo annihilation at a slower pace (figure 6); because of reversal of the curvature of the threads their self-induction is not such as to keep them pressed against each other. In fact the two threads now move apart (compare figures 4f, 4g), their separation is smallest at the center where they are straight and larger near the ends where they are more curved (hence have higher self-induction away from each other). The reversal of the curvature of the threads and their moving apart would arrest annihilation, but the axial stretching of the threads intensifies their vorticity and thus sustains their annihilation by cross-diffusion, although at a slower pace. Note that at $t = 6$, the threads appear pinched off from the bridges. The picture is not totally clear; there appears to be complex entanglement of the thread ends around the bridges. The details of the entanglement are clearly not captured by the resolution in our simulation.

The simulation is terminated at $t = 6$ because beyond this time the vortices in the neighboring cubes start affecting the flow. Also, since the threads decay slowly at viscous time scales no further significant changes are expected. The two reconnected crescent-shaped vortices (essentially halves of vortex rings connecting across the boundary, which would evolve little from now on) taper off at the boundary at the $|\omega|$ level plotted, presumably because the vorticity is highly diffuse at the boundary; thus there is no vorticity at the level plotted.

While the threads are slowly decaying, there is a possibility that the thread pair may undergo a second-level cut-and-connect. This can happen if a perturbation reverses the dipole motion in the contact zone. It can also happen without a perturbation due to the fact that the middle portion of the threads can reverse curvature, once again, by mutual induction. Then self induction will pull the two threads closer to each other to enhance annihilation, reconnection and formation of "bridglets". Thus, this second cross-linking may constitute a second stage in a sequence of cut-and-connect interactions—a fascinating cascade mechanism!

The cut-and-connect generates orthogonal vorticity. The threading, or even successive cascade of cross-linking, would produce finer scales of vorticity with progressive increase of vorticity surface and decrease in scale. This may lead to enhanced mixing. The progressive fine scale generation would be a new and interesting enstrophy cascade mechanism. As we have claimed that cut-and-connect happens continually in all turbulent flows, we have here a non-statistical explanation for mixing and enstrophy cascade.

Figure 6(a) suggests three characteristic time scales of the phenomenon. Phase I: $0 < t < t_1$, where t_1 is the approach time during which circulation remains virtually constant while vorticity increases sharply. Phase II: $t_1 < t < t_2$, during which most annihilation takes place. Phase III: $t > t_2$, the period of decay of threads. These three phases can be identified by drawing a straight line tangent to the $\Gamma(t)$ curve through the point of inflection (figure 6b). The point where this tangent intersects the $\Gamma(0)$ line defines t_1. The determination of t_2, however, is not so precise as the decay curve slope is not well defined for the duration of the simulation. We estimate for this simulation $t_1 \approx 2.7$ and $t_2 \approx 4.3$. Using these two times, one can define the reconnection time as $t_r = t_2 - t_1 = 1.6$. This value compares favorably with Schatzle's (1987) time scale $\sigma^2/(\Gamma\nu)^{\frac{1}{2}} \approx 1.7$, while the time scale $\sigma^2/\Gamma \approx .05$ proposed by Takaki & Hussain (1985) is too fast. We also note that the viscous time scale $\sigma^2/\nu \approx 55$ is too long. We expect the reconnection time to decrease with Re; hence, the Takaki-Hussain time scale may be more appropriate at high Re.

We also followed the evolution of a passive scalar for the case of unit Schmidt number. This scalar was put in one vortex only, and in this vortex the scalar was set equal to the vorticity magnitude. At $t = 6$, we found virtually no scalar in the threads and very little in the bridges. Where vorticity is enhanced by stretching, markers are depleted; thus visualization may divert our attention away from most interesting points in a flow.

4. Discussion

4.1. *Bridging: the essence of vortex cross-linking*

We claim that bridging is the essence of cross-linking and is a simple consequence of vorticity annihilation. That is, all cross-linking must involve bridging. When vortices collide in a nonparallel manner other facets of interaction such as entanglement and filamentation may mask bridging, but it is the central mechanism by which vorticity cross-linking happens. Here we delineate the mechanism and suggest possible modeling of it.

Consider the two antiparallel vortex tubes (figure 7a) with three vortex lines each, emanating from three fluid particles in the main core. Viscous cross-diffusion annihilates the innermost vortex lines along the contact zone. This would leave the two innermost vortex lines devoid of their central parts, were it not the case that the remainder of these vortex lines link-up or connect near each end of the contact zone (figure 7b). The pumping (i.e. swirl) of the vortex tubes advects this reconnected vortex line upward, while simultaneously, vorticity diffusion across the tip of the narrow cusp (the reconnection point) makes the tip recede so that the tip radius of curvature increases from zero (figure 7c). The advection of the cusp is arrested as it approaches the stagnation point in front of the vortex dipole. In parallel, the swirl of the tubes stretch the vortex line and further increases the radius of curvature at the cusp (figures 7d,e). The continual stretching of the vortex line 'straightens out' the kink as the line is wrapped around the two tubes (figure 7f). Where the cusp disappears (i.e., whether the cusp disappears before arrival at the stagnation point) depends on the ratio of the advection time to diffusion time, hence

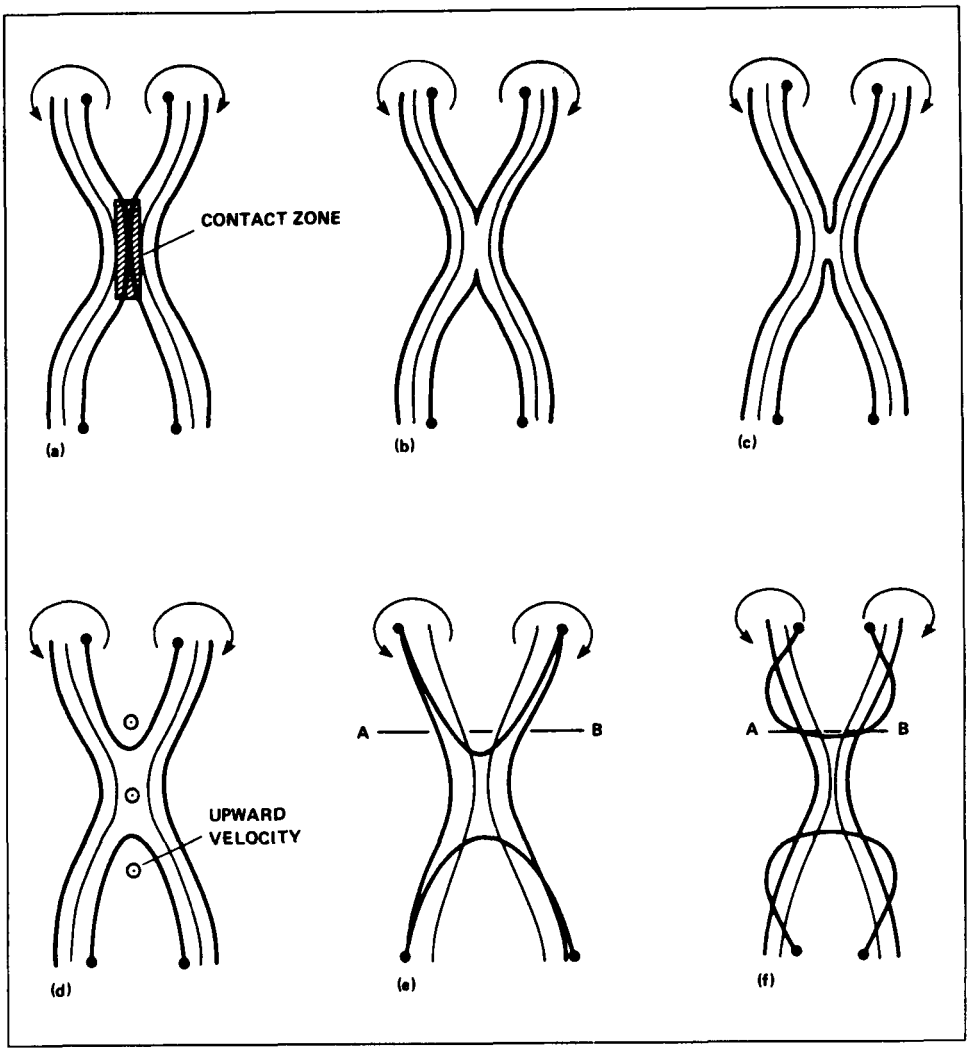

FIGURE 7. (a–f) schematic of annihilation and reconnection.

Re. This is how one sees *Re* entering directly into the discussion and modelling of the phenomenon. It should be obvious how successive reconnected vortex lines pile up at the stagnation points to form bridges.

To further understand the bridging mechanism, let us now consider the cross-section AB in figures 7(e) and 7(f). Drawn in figure 7(g), this cross-section shows the dipole structure of the antiparallel vortex tubes. In a reference frame moving with this dipole the streamline patterns have two stagnation points: S_T and S_B. It is now clear that our reconnected vortex line comes to a rest near the front stagnation point S_T. This point being a saddle, the vortex line is subject to continued stretching along the diverging separatrix a–a.

This scenario illustrates how reconnected vortex lines appear on the top of the

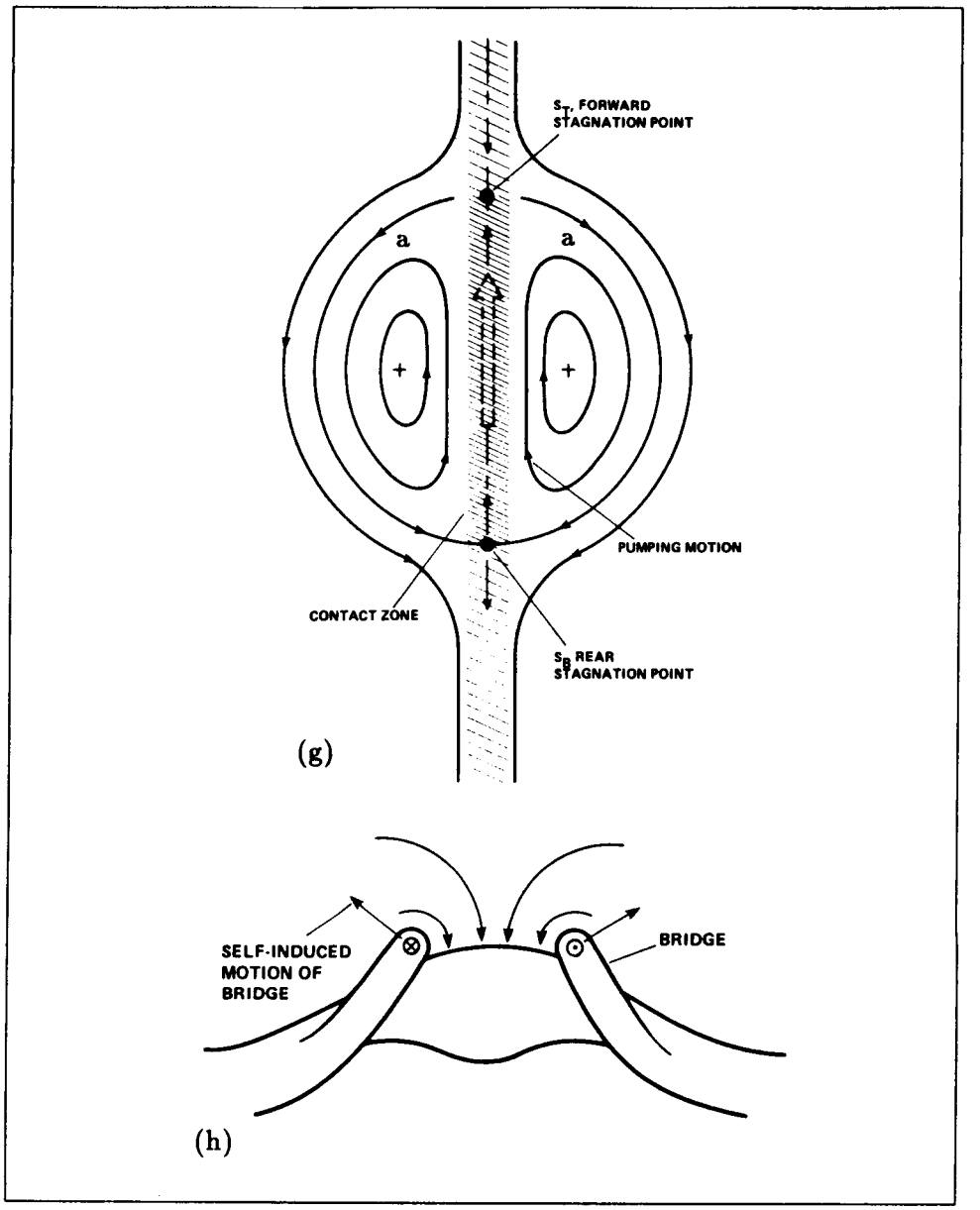

FIGURE 7. (g) streamline pattern in the xy-plane showing stagnation points S_T and S_B; (h) bridging showing self-induced motion of the bridge (straight arrows) and velocity induced on the threads (curved arrows).

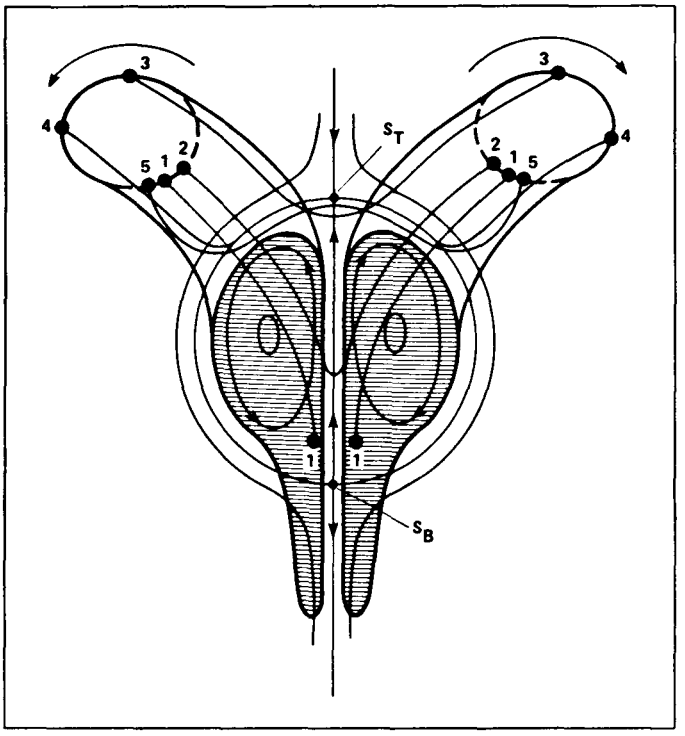

FIGURE 8. Advection and accumulation of reconnected vortex lines forming bridges. The streamline pattern of 7(g) is superimposed on the vorticity contours (hatched area). Lines 1-1, 2-2, 3-3, 4-4 and 5-5 represent successive positions of a vortex line.

antiparallel vortex tubes and get aligned orthogonally i.e. along a–a. Figure 7g also shows that as the reconnected vortex fluid is pumped to S_T, the contact zone (marked by hatches with intensity intended to denote local rate of annihilation) continuously gets supplied with fresh vortex lines starting essentially from near the back stagnation point S_B. The effect of this mechanism is an accumulation of the newly-linked vortex lines at S_T along a–a, thereby explaining the 'humps' we observe on top of the antiparallel vortices in the wire plots (figure 3e). The motion of the bridges due to self induction and the flow induced by them are illustrated in figure 7(h).

The process is schematically explained in the perspective view of one half of the two vortices in figure 8. The figure depicts vortex lines emanating from a fluid particle located at points numbered 1–5 at successive instants.

Figure 9 is a cross-sectional view of the dipole, showing both streamlines (in the frame advected with the dipole) and zones of vorticity. The streamlines show how fluid marked by annihilated vorticity (hence also the tips of the reconnected vortex lines) is advected away from in between the two vortices (dipole) to the stagnation point as the connection point recedes by both diffusion and stretching.

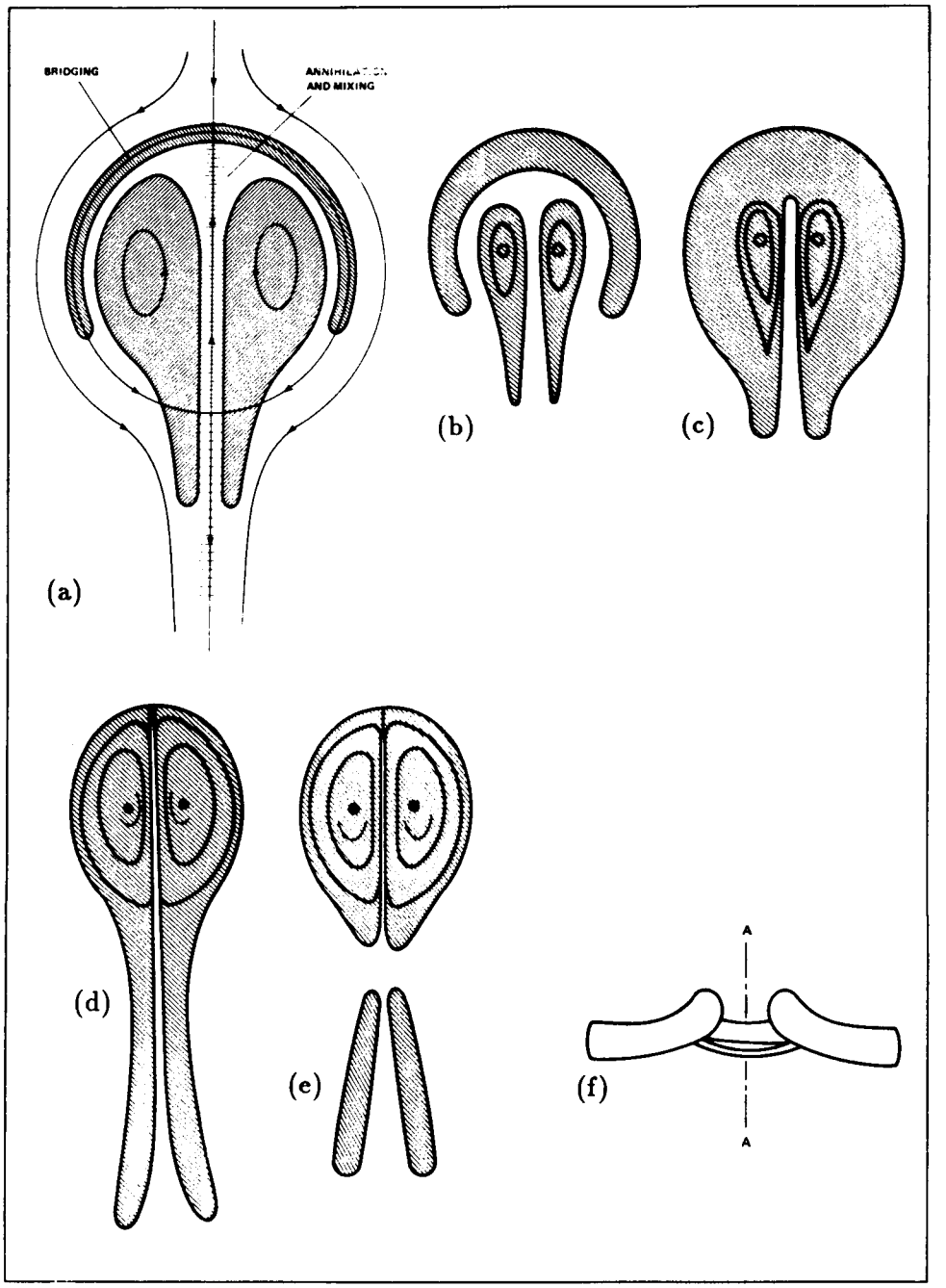

FIGURE 9. (a–f) Motion in dipole and vorticity field in a plane parellel to the xy-plane and passing through the bridges. The configuration (c) results from (b) after fusion of the shroud with the eyes. The head-tail structure is shown in (d) before the head detaches from the tail in (e), which is the cross-section A–A in (f).

The cross-section, as viewed in $|\omega|$ contours, then takes a shape shown in figure 9(b). The characteristic structure of a head-tail dipole with a top shroud (the shroud containing vorticity orthogonal to that of the two "eyes") undergoes changes as the "eyes" are continually depleted due to annihilation and the shroud, which represents a bridge, becomes heavier (due to accumulation of newer vortex lines). Simultaneously, as a result of viscous diffusion the shroud fuses with the dipole into a single structure (figure 9c).

As the reconnected vortex lines accumulate near S_T, so that the bridges acquire a circulation comparable to that of the antiparallel vortex tubes, a new phase of the evolution begins. The bridges (now looking like curved hairpins) begin to move away from each other by self-induction, and also initiate a downwash in the contact zone (figure 7h). This downwash soon becomes strong enough to dominate the upward motion of the dipole in the symmetry plane. There are two reasons for this; first, the circulation in the bridges grows; second, the dipole acquires a head-tail structure and only the vorticity in the head is responsible for the upward motion (figure 9d). Mutual induction causes the heads to move ahead leaving the tail behind to undergo uneventful viscous decay. This is shown in figure 9(e) which represents the section A–A in figure 9(f) representing the state at $t = 4.5$ (figures 3f, 4f). The downwash causes the curvature of the antiparallel vortices to reverse. The antiparallel vortices will therefore no longer be pushed towards each other by self-induction; on the contrary, self-induction will now tend to push the vortices apart. The primary cause of continued fast annihilation is therefore disappearing. This explains why the cut and connect is only partial. The slender threads, which are the remnants of the original vortex tubes, disappear on a longer and qualitatively different time scale.

Regarding accumulation of reconnected vortex lines, the vorticity contours in the yz plane show interesting features (figures 5a–d). As seen from figure 7, new (reconnected) vortex lines are drawn in the bridges from the contact zone, as the bridges continue their swirl. In figure 5b the right hand side bridge moves counterclockwise and the left hand side one moves clockwise. As more and more vortexlines are accumulated, the bridge core starts to become rounded. The peak vorticity is not at the center but toward the side to which the bridges are being advected by mutual and self induction.

4.2. *Modeling of cross-linking, bridging and threading*

In spite of extensive current interest in the cut-and-connect mechanism, its understanding is poor. Less satisfactory is its modeling. We emphasize that one must translate observations—numerical and experimental—into an analytical, at least conceptual, model. In this section we discuss how the insights that we have obtained may be used to construct a model for the crucial stage II, namely, bridging. We shall merely provide the conceptual framework of our model and hope to treat analysis in the future. We draw upon well-understood and simple vortex situations and try to keep the model two-dimensional, at least locally.

There are four principal ingredients of our qualitative description of the cross-linking mechanism in phase II. These are : (i) self-induction due to curvature, (ii)

stretching (by mutual induction) and core deformation, (iii) evolution of two orthogonal vortex dipoles: one in the symmetric plane and the other in the dividing plane, and (iv) annihilation of antiparallel vortex lines by cross-diffusion. Of these, core deformation and cross-diffusion seem to be most difficult to model accurately. Both effects are coupled to the details of the vorticity distribution within the cores: diffusion is the strongest in regions of large gradients and core deformations produce complicated regions of gradient intensification (Melander *et al.* 1987). We concentrate on adequately modeling these two effects, ignoring for the time being 3D details which we consider less important. In this framework, we limit our consideration to the two orthogonal planes—the symmetric and dividing planes—hoping to use the simple 2D evolution equations in each plane, that are coupled together to model 3D effects. The 3D effect is included by incorporating local curvature of the vortices. The bridges are nonplanar so that curvature varies continuously in direction and magnitude along the vortex. We shall make the assumption, however, that curvature is constant along a vortex, although a function of time.

At the end of phase I (inviscid advection), the two vortex tubes touch each other with a contact zone that extends from C_1 to C_2 as shown in two orthogonal views in figures 10(a) and 10(b) and perspective view in 10(c). The cross-linked vortex-lines $C_1'C_1''$ and $C_2'C_2''$ lying within the bridges have radius of curvature r_b at the intersection of the bridges with the dividing plane. Their binormals $\mathbf{b}_{C_1}$ and $\mathbf{b}_{C_2}$ at C_1 and C_2 are in the dividing (yz) plane, but parallel to neither the z nor y axis. In the symmetric plane (figure 10b), vortex tubes have a radius of curvature r_c and the binormal $\mathbf{b}_c$ is in the x direction. We assume for modeling purposes that r_b, r_c, $\mathbf{b}_{C_1}$, $\mathbf{b}_{C_2}$ depend only on time.

In our simplified model the interaction zone consists of two orthogonal dipoles. Let us call the dipole formed by the bridges as the *growing* dipole and the one formed by the initial annihilating vortex tubes as the *dying* dipole. The treatment of the dying dipole is 2D but allows for: i) curvature effects, ii) stretching in the z direction (figure 10d), and external velocity field $\mathbf{v}_b$ due to the bridges or growing dipole (figure 10c). The x-dependence of $\mathbf{v}_b$ is not strong near $x = 0$. Thus we can take the $\mathbf{v}_b$ field from the yz plane and assume it to be constant across the dying dipole. The axial stretching $S_z = \partial w_b/\partial z$ of the dying dipole can accordingly be assumed to be that in the yz plane. To consider the time evolution of the radius of curvature r_c, we assume that the tubes remain parallel (i.e., they remain pressed against each other) and their mutual induction is constant along the length, so that the change of curvature is only due to z-variation of $\mathbf{v}_b$. By symmetry $\partial v_b/\partial z = 0$. Hence r_c is determined by $\partial^2 v_b/\partial z^2$. However, since $\mathbf{v}_b$ is a function of z and y, assuming that we focus our attention on $z = 0$, we must specify the position along the y-axis where $\partial^2 v_b/\partial z^2$ should be evaluated. The centroid location of the decaying dipole is the clear choice. With these approximations we may write equations for the dying dipole; these equations depend only on the flow in the dividing (yz) plane.

How do we model the growing dipole? As vorticity is being annihilated (in the

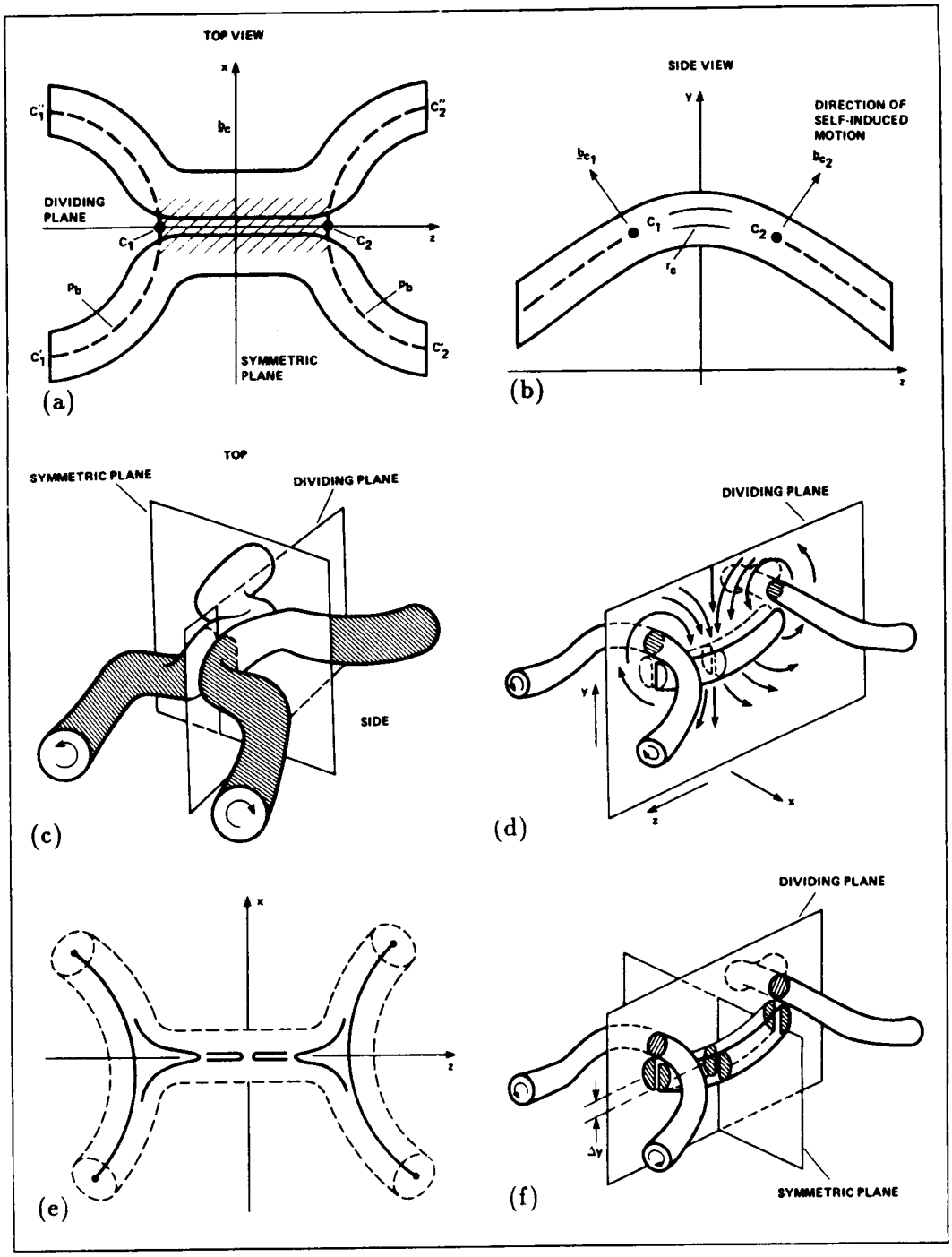

FIGURE 10. Modeling of the reconnection, bridging and threading. The cross-linking zone is shown is shown in top view (a), side view (b) and perspective view (c). The growing dipole is illustrated in (d). The receding of vortex lines during annihilation and cross-linking is shown in (e). The curvature of threads and their modeling is shown in (f).

dying dipole) by cross-diffusion, we immediately feed an equivalent amount of microcirculation into the growing dipole i.e. to the bridges. A crucial question is at what location should this microcirculation be added in the dividing plane. Since vortex lines in the contact zone are nearly antiparallel, we assume an instant annihilation throughout the entire length of the contact zone. In reality, the process is a progressive, though quick, retreat, as shown in figure 10(e). The z-coordinate for the addition of microcirculation is thus clear, namely, the end points C_1 and C_2 of the contact zone. At what y? Let us assume that the dying dipole under the bridges is exactly the same as in the symmetric plane (figure 10e) except that it is displaced in y by Δy due to curvature r_c (thus Δy is known when the distance between the bridges i.e. between C_1 and C_2 is known). The midpoint of this dipole (i.e. point d) denotes the y-location for addition of microcirculation. In other words, the y-location for addition of microcirculation equals the y-location for annihilation plus Δy. The advection of this microcirculation from d to C_1 depends on the strength of the dying dipole. Once again, C_1 and C_2 are the centroids of the bridges in the dividing plane. How the binormals $\mathbf{b}_{C_1}$ and $\mathbf{b}_{C_2}$ evolve is not clear to us yet, but we believe we have here an outline of a reasonable cross-linking model.

The model thus gives evolution equations for two 2D problems with initial conditions given by phase I. The advantage of this model is that we avoid making any assumption regarding core deformation and annihilation, which are two most crucial parts of the process. The disadvantage is that inaccuracies may result from the fact that we have made strong assumptions on the overall 3D structure of the process. However, these assumptions are motivated by our observations.

4.3. *Effect of asymmetry*

The simulation with initial asymmetries produced virtually the same pictures of vorticity wire plots as in figures 3(a–g). At $t = 6$, the plot is virtually indistinguishable from that shown in figure 3(g). We conclude that the phenomenon is insensitive to small asymmetries as long as the vortices are of equal circulations and the analysis (Takaki & Hussain 1985) and high-resolution simulation (Kerr & Hussain 1988) involving symmetry are appropriate for studying the phenomenon.

4.4. *Re dependence*

In order to obtain some idea of the dependence on Re, another simulation for $Re(= \Gamma/\nu) = 500$ was performed. Plots of $|\omega|$ are shown in figures 11(a–h). A similar evolution is seen as at $Re = 1000$ except that at $t = 6$ the reconnection is at an earlier stage. Note that the vorticity level in figures 11 (a–e) are those of figure 3 (i.e., 30% of the initial peak value). At this lower Re, vorticity diffuses more; thus a lower vorticity level is required for capturing the details.

See figures 11(f–h) for vorticity surfaces at the 15% level. We conclude that while time is not scaled properly (which is not unexpected) the mechanisms present are the same. It is particularly interesting to note that two orthogonal dipoles are clear in figures 11(d,e).

5. Other topological properties

The 3D direct simulation of the Navier-Stokes equation provides considerable

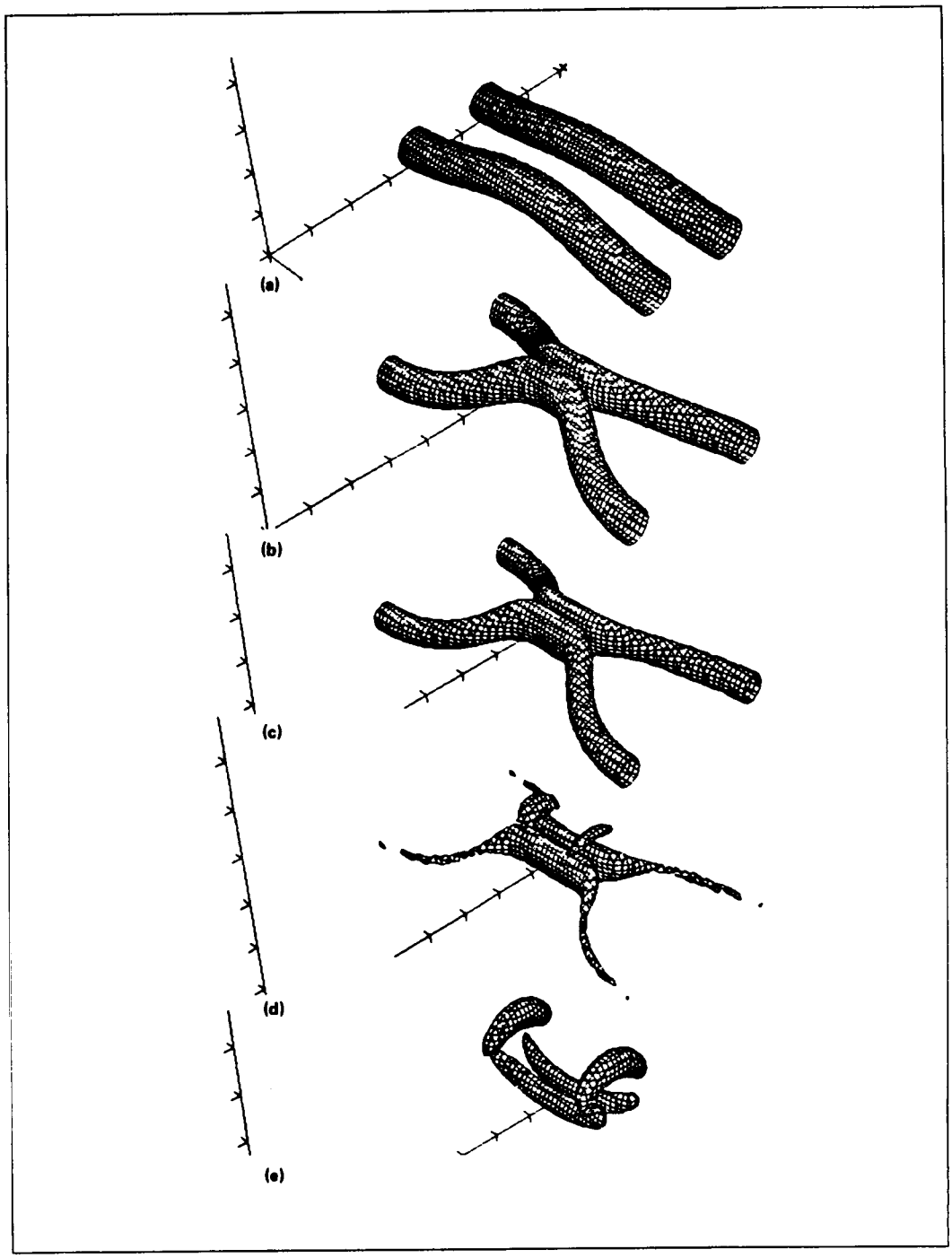

FIGURE 11. Wire plots of $|\omega|$ at 30% of initial peak vorticity at t =0,3,3.75,4.5 and 6, respectively.

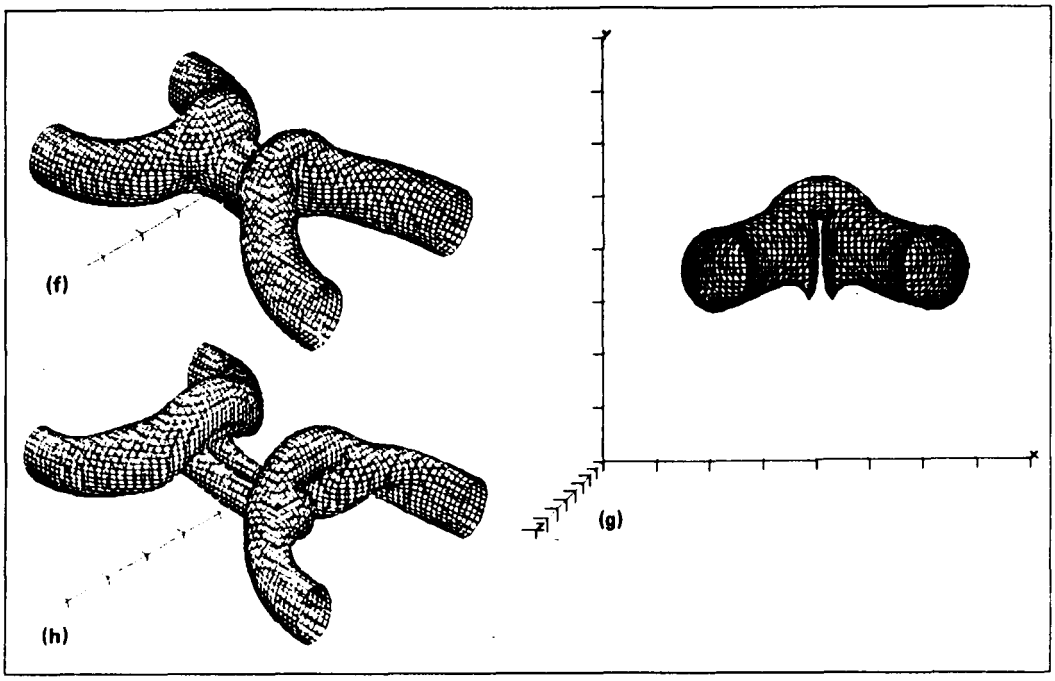

FIGURE 11. (f–g), two views of $|\omega|$ surface at 15% of initial peak vorticity at t =4.5; (h), same as (f) but at t =6.

amount of spatial data unavailable experimentally. These provide the researcher valuable information regarding the topology and dynamics of the interacting vortices. While post-processing and visual examination on graphic stations proves extremely illuminating, information gathered visually is typically overwhelming and has to be properly synthesized and interpreted. More challenging is the selection of appropriate flow fields, the inspection plane or view, property of interest and contour levels to optimally capture a time-changing dynamical event in a turbulent flow. We did not have adequate time for this phase and thus present here a few select examples of topological properties during the reconnection process.

The approach undertaken here is similar to the ones employed by us for the study of coherent structures in turbulent shear flows (See for example Hussain 1980, 1983, 1986). Of the variety of properties that can be useful in studying the topology and dynamics, we limit our attention to scalar intensity c, enstrophy production $P_s = \omega_i s_{ij} \omega_j$, dissipation $\epsilon = 2\nu s_{ij} s_{ij}$ and helicity density $h = u_i \omega_i$. We will present here only a few examples. The contours of dissipation are shown for the symmetry (xy) plane in figure 12(a–e) for $t = 2, 3, 3.75, 4.5$ and 6, and for the dividing (yz) plane in figure 12(f–i) for $t = 2, 3, 3.75$ and 4.5, respectively.

In order to focus on specific details, we choose one instant, namely, $t = 4.5$. Figure 13 shows enstrophy production.

Dissipation and helicity are shown in figures 14 and 15 at 20% and 50% of their peaks values. The perception of the details depends considerably on the contour

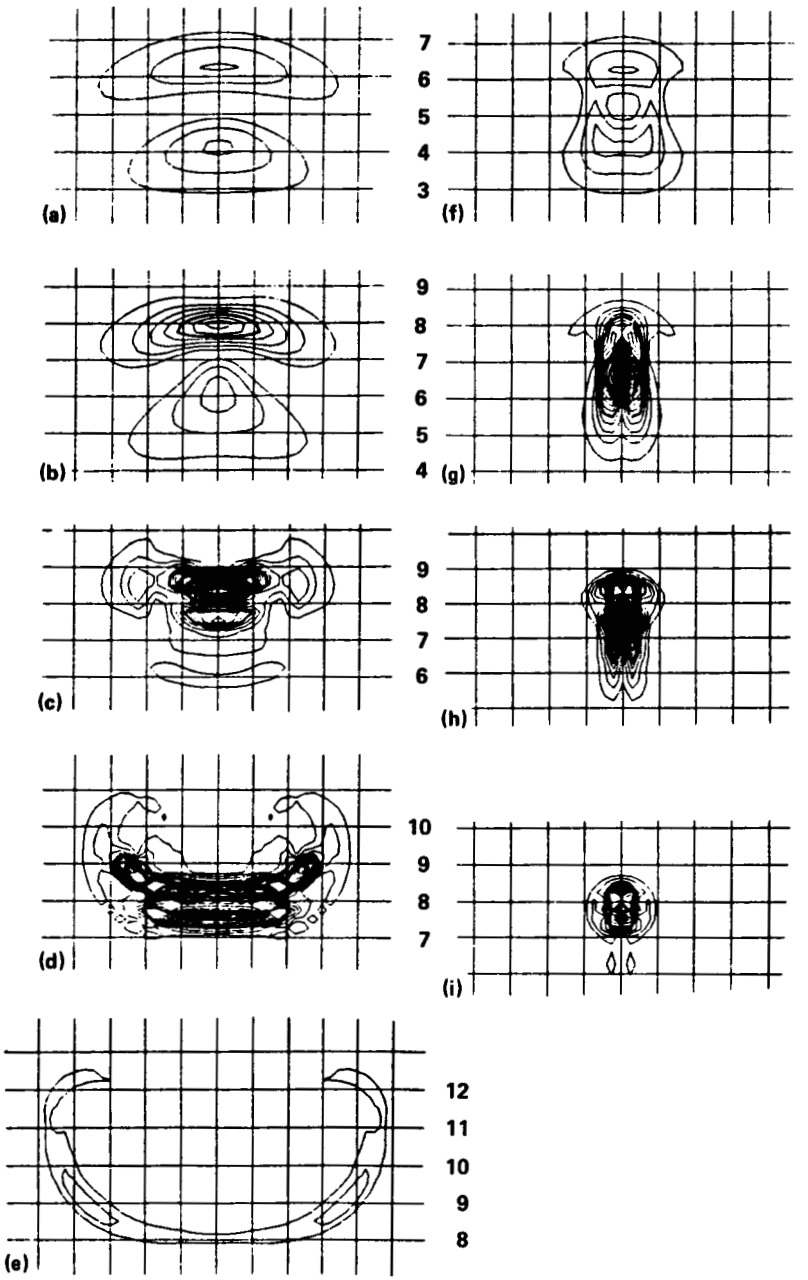

FIGURE 12. Contours of kinetic energy dissipation rate. (a–e), yz-plane at t =2,3,3.75,4.5 and 6, respectively; (f–i), xy-plane at t =2,3,3.75, and 4.5, respectively. The grid is four times coarser than the computational mesh. The numbers on the right serve to indicate the y locations.

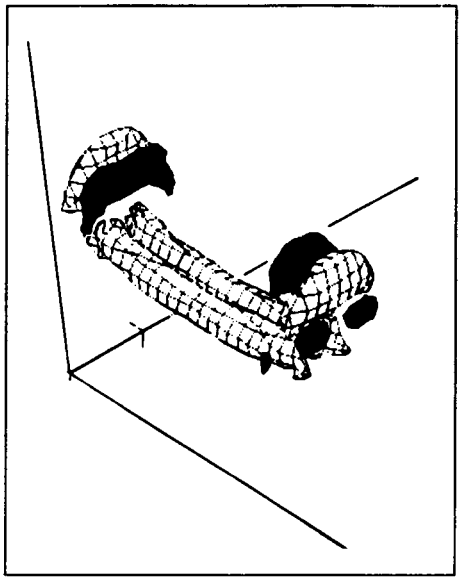

FIGURE 13. Surface contours of enstrophy production at $t = 4.5$. Black, negative production at 20% of the peak negative value; hatched, positive production at 20% of the peak positive value. The magnitude of the positive peak is about twice as large as the negative peak.

level. The correspondence between cross-sectional and projected views (for example, compare 12d and 14) is not obvious. One must examine the entire flow field; however, space does not permit comprehensive documentation. Below, we only summarize our observations without including additional figures.

Not surprisingly, enstrophy production occurs mostly in the contact zone and threads and somewhat in the bridges but in complicated way. For instance figure 13 shows that in the bridges there is both positive and negative production corresponding to vorticity stretching and compression, respectively. For most of the remaining regions, there is very little production, except that there are large regions of low-level *negative* production. This is because self induction produces slight compression and fattening of the vortices (see figure 3). This is consistent with the observed accumulation of scalar, as well as progressive fattening of the scalar domain, in the same regions.

Within the dipole, dissipation mostly occurs in a small region containing the contact plane (figures 12f–i) but significant dissipation is also present above the contact zone around the forward stagnation point. We find the peak to lie near the intersection of the two symmetry planes. Since helicity density vanishes in these planes by symmetry, the peaks of dissipation and helicity density are mutually exclusive. There is significant helicity generation where the threads wrap around the bridges (figure 15). The high helicity density in the threads (figure 15b) suggests long life—consistent with our observation that the threads decay very slowly.

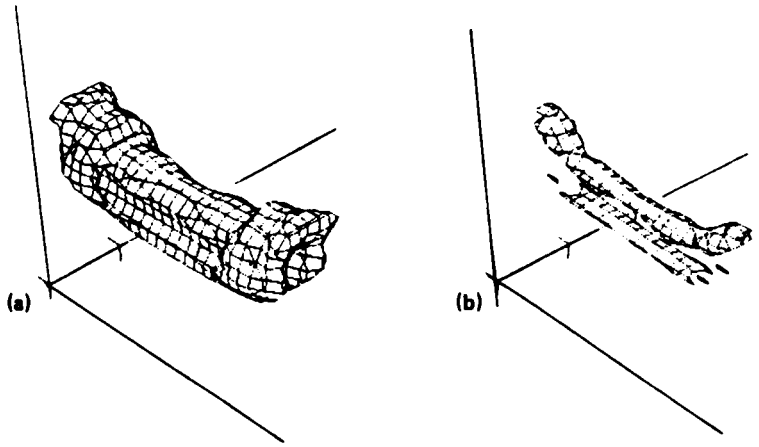

FIGURE 14. Surface contours of dissipation at $t = 4.5$. (a) 20% level; (b) 50% level.

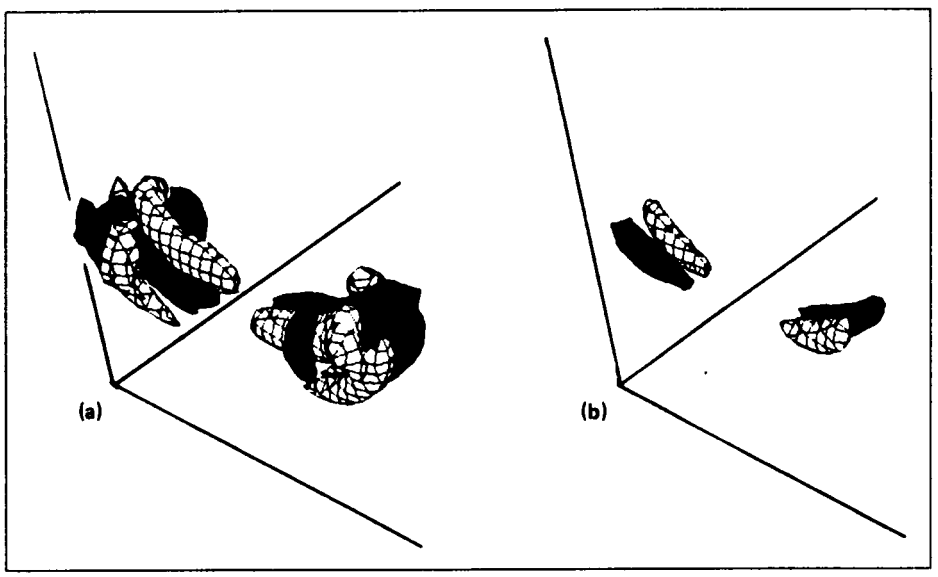

FIGURE 15. Contours of helicity density at $t = 4.5$. (a), 20% of peak negative (black) and positive (hatched); (b) 50% levels as in (a).

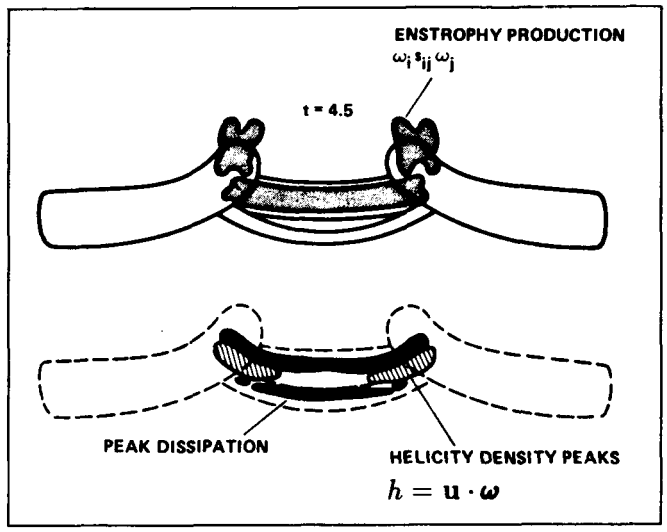

FIGURE 16. Comparison between regions of large enstrophy production, helicity density and dissipation at $t = 4.5$.

The possible correspondence between dissipation and helicity has been of particular interest in studies of turbulent flow. Hussain (1986) suggested that contrary to claims elsewhere (Moffatt 1985; Tsinober & Levich 1983) the domains of helicity and dissipation cannot be spatially independent even though the peaks may be. The present data are consistent with this view (see figure 16).

When we compare the scalar field with vorticity (for computation with unit Schmidt number) we find that they are rather different. In particular, the bridges have no scalar. This can be explained by the fact that vorticity stretching is accompanied by corresponding decrease of specie concentration. We have persistently warned against the use of flow visualization for study of coherent structures and vorticity field in turbulent or unsteady flow and warned that the difference is not due to non-unity Schmidt number alone (Hussain 1980, 1983). The present simulation clearly supports our warning.

6. Concluding remarks

Vortex interactions involving cross-linking consist of four phases: (0) antiparellelization, (i) core flattening and stretching, (ii) bridging, and (iii) threading. Since the first was observed in various numerical simulations and is consistent with Biot-Savart induction, we focused on the latter three phases. The choice of antiparallel vortices has eliminated distracting complexities that result in the case of collision at arbitrary orientations. The simulation not only has shed considerable light on the heretofore unknown details of the mechanism but also helped us provide a conceptual model. The most significant outcomes of this study are the discovery and explanation of the bridging process and the fact that cross-linking is incomplete. The formation of long-lived threads clearly play some role in enstrophy cascade and

mixing. These threads decay at viscous time scale due to the formation of head-tail structure and the reversal, induced by the bridges, of the curvature of the vortex dipole. The simulation has also vividly demonstrated that vorticity field can be different from scalar field even in the case of unity Schmidt number. The phenomenon is clearly the same at different Re while the reconnection time is *Re* dependent.

This simulation is a first attempt at understanding the reconnection mechanism. But more information is needed regarding the details of the topology change and *Re* effect. We need higher *Re* simulations with finer resolution before finer analysis can be attempted. Considering inherent limitation of even the supercomputer capability, invoking symmetry seems unavoidable. Simulations and analysis invoking symmetries, which were viewed with skepticism by many researchers, are now vindicated.

As hard as it is, we must obtain detailed 3D experimental data, beyond those provided by Schatzle's experiments. It is through a close collaboration between experiments and simulation that a clearer understanding and modeling of this phenomenon will emerge. We are planning such collaborative research involving high-resolution simulation and experiments.

This research was mostly performed during the 1988 summer term of the CTR. We are thankful to K. Shariff and P. Moin for illuminating discussions. In addition, F.H. acknowledges the support of ONR Grant N00014-87-K-0126.

REFERENCES

ANDRECK & GLABERSON 1982 Tkachenko waves. *J. Low Temp. Phys.* **48**, 257–296.

AREF, H. 1982 Integrable, chaotic, and turbulent vortex-motion in two-dimensional flows. *Ann. Rev. Fluid Mech.* **15**, 345–389.

ASHURST, W.T. & MEIRON, D.I. 1987 Numerical study of vortex reconnection. *Phys. Rev. Lett.* **58**, 1632–1635.

BATCHELOR, G.K. 1967 *An Introduction to Fluid Dynamics*.Cambridge University Press: Cambridge, England.

BENJAMIN, T.B. 1985 Private communication.

CANTWELL, B.J. 1981 Organized motion in turbulent flow. *Ann. Rev. Fluid Mech.* **13**, 457–515.

CROW, S.C. 1970 Stability theory for a pair of trailing vortices. *AIAA J.* **8**, 2172–2179.

HOPFINGER, E., BROWAND, F.K. & GAGNE, Y. Turbulence and waves in a rotating tank. 1982 *J. Fluid Mech.* **125**, 505–534.

HUSSAIN, F. & HUSAIN, H. 1987 Passive and active control of jet turbulence. In *Turbulence Management and Relaminarization* (ed. H. Liepman & R. Narasimha), pp. 445–457, Springer Verlag: New-York, Heidelberg, Berlin.

HUSSAIN, A.K.M.F. 1980 Coherent structures and studies of perturbed and unperturbed jets. In *The Role of Coherent Structures in Modelling Turbulence and Mixing* (ed. J. Jimenez), Lecture Notes in Physics, vol. 136, pp. 252–291, Springer Verlag: New-York, Heidelberg, Berlin.

HUSSAIN, A.K.M.F. 1983 Coherent structures–reality and myth. *Phys. Fluids* **26**, 2816–2850.

HUSSAIN, A.K.M.F. 1986 Coherent structures and turbulence. *J. Fluid. Mech.* **173**, 303–356.

KAMBE, T. & MINOTA, T. 1983 Acoustic wave radiated by head-on collision of two vortex rings. *Proc. R. Soc. Lond.* A **386**, 277–308.

KERR, R.M. & HUSSAIN, F. 1988 Simulation of vortex reconnection. *Physica* D, Submitted.

KIDA, S. & TAKAOKA, M. 1987 Bridging in vortex reconnection. *Phys. Fluids* **30**, 2911–2914.

KIDA, S., TAKAOKA, M. & HUSSAIN, F. 1988 Reconnection of two vortex rings. *Phys. Fluids*, Submitted.

KIM, J. & MOIN, P. 1986 The structure of the vorticity field in turbulent channel flow. Part 2. Study of ensemble averaged fields. *J. Fluid Mech.* **162**, 339–363.

LAUFER, J. 1974 On the mechanism of noise generation by turbulence. In *Omaggio a Carlo Ferrari*, Liberia editrice universitaria levrotto & bella Torino, 451–464.

LEONARD, A. 1980 Vortex methods for flow simulation. *J. Comp. Phys.* **37**, 289–335.

LUMLEY, J. 1981 Coherent structures in turbulence. In *Transition and Turbulence* (ed. R.E. Meyer), pp. 215–242, Academic Press: New York.

MEIRON, D.I., SHELLEY, M.J., ASHURST, W.T. & ORSZAG, S.A. 1988 Numerical study of vortex reconnection. *Physica D*, Submitted.

MELANDER, M.V., ZABUSKY, N.J. & STYCZEK, A.S. 1986 A moment model for vortex interactions of the two-dimensional Euler equations. Part 1. Computational validation of a Hamiltonian elliptical representation. *J. Fluid Mech.* **167**, 95–115.

MELANDER, M.V., MCWILLIAMS, J.C. & ZABUSKY, N.J. 1987 Axisymmetrization and vorticity-gradient intensification of an isolated two-dimensional vortex through filamentation. *J. Fluid Mech.* **178**, 137–159.

MELANDER, M.V. & ZABUSKY, N.J. 1988 Entanglement produces an apparent reconnection of 3D vortex tubes. *Phys. Rev. Lett.*, Submitted.

MELANDER, M.V., ZABUSKY, N.J. & MCWILLIAMS, 1988 Symmetric vortex merger in two dimensions: causes and conditions. *J. Fluid Mech.* **195**, To appear.

MOFFATT, H.K. 1985 Magnetostatic equilibria and analogous Euler flows of arbitrarily complex topology. Part 1. Fundamentals. *J. Fluid Mech.* **159**, 359–378.

MOIN, P., LEONARD, A. & KIM, J. 1986 Evolution of a curved vortex filament into a vortex ring. *Phys. Fluids* **29**, 955–963.

OSHIMA, Y. & ASAKA, S. 1977 Interaction of two vortex rings along parallel axes in air. *J. Phys. Soc. Jap.* **42**, 708–713.

PUMIR, A. & SIGGIA, E.D. 1987 Vortex dynamics and the existence of solutions to the Navier-Stokes equations. *Phys. Fluids* **30**, 1606–1626.

SAFFMAN, P.G. 1978 The number of waves on unstable vortex rings. *J. Fluid Mech.* **84**, 625–639.

SCHATZLE, P.R. 1987 An experimental study of fusion of vortex rings. Ph.D. Thesis, Graduate Aeronautical Laboratories, Calif. Inst. Tech.

SCHWARZ, K. 1985 Three-dimensional vortex dynamics in superfluid ^{4}He: Line-line and line-boundary interactions. *Phys. Rev.* B **31**, 5782–5804.

SIGGIA, E.D. 1985 Collapse and amplification of a vortex filament. *Phys. Fluids* **28**, 794–805.

SIGGIA, E.D. & PUMIR, A. 1985 Incipient singularities in the Navier-Stokes equations. *Phys. Rev. Lett.* **55**, 1749–1752.

STANAWAY, S.K., SHARIFF, K. & HUSSAIN, F. 1988 Head-on collision of viscous vortex rings. In Proceedings of the 1988 Summer Program, Center for Turbulence Research.

TAKAKI, R. & HUSSAIN, F. 1984 On the dynamics of entangled vortex filaments. *Phys. Fluids* **27**, 761–763.

TAKAKI, R. & HUSSAIN, A.K.M.F. 1985 Recombination of vortex filaments and its role in aerodynamic noise. In *Proc. Fifth Symposium on Turbulent Shear Flows*, pp. 3.19–3.25.

TSINOBER, A. & LEVICH, E. 1983 On the helical nature of three-dimensional coherent structures in turbulent flows. *Phys. Lett.* A **99**, 321–324.

WIDNALL, S.E., BLISS, D.B. & TSAI, C.-Y. 1974 The instability of short waves on a vortex ring. *J. Fluid. Mech.* **66**, 35–47.

ZABUSKY, N.J. & MELANDER, M.V. 1988 Three dimensional vortex tube reconnection: morphology of orthogonally-offset tubes. *Physica* D, Submitted.